Linear momentum transfer and light particle emission in the $E/A = 25$ MeV ^{6}Li + ^{238}U reaction

M. Fatyga, H. J. Karwowski,* K. Kwiatkowski, L. Nowicki,† and V. E. Viola
Departments of Physics and Chemistry and Indiana University Cyclotron Facility, Indiana University, Bloomington, Indiana 47405

K. Hicks‡
Department of Physics, University of Colorado, Boulder, Colorado 80309
(Received 25 August 1986)

Inclusive measurements of the linear momentum transfer distribution and exclusive studies of light-charged particles as a function of linear momentum transfer have been performed for the reaction of 150-MeV ^{6}Li ions with ^{238}U. Linear momentum transfer properties and an upper limit for the complete fusion cross section for this system were deduced from the folding angle between binary fission events and found to be consistent with data for heavier complex projectiles. The exclusive light-charged-particle data demonstrate the existence of fission following the transfer of all possible subdivisions of the ^{6}Li projectile, as well as inelastic scattering. Absorptive breakup involving ^{4}He-^{2}H cluster structure is found to be the dominant reaction mechanism. In addition, substantial yields of energetic protons associated with full linear momentum transfer are observed in the backward hemisphere. However, the temperature inferred from these spectra is nearly three times as large as that for a fully equilibrated compound nucleus, suggesting a nonequilibrium source for these particles.

I. INTRODUCTION

The study of nonequilibrium processes in nucleus-nucleus collisions has received a major stimulus recently from the availability of high quality beams of intermediate-energy projectiles. Many models have been proposed to explain the energetic particle spectra, strongly forward-peaked angular distributions, and multibody final states associated with the spectrum of ejectiles observed in these energetic collisions. Among these are the exciton model,[1] intranuclear cascade codes,[2,3] coalescence approaches,[4] and local thermodynamic models.[5] Although calculations based on these models are able to reproduce some average properties of these reactions reasonably well, none can provide a quantitative, self-consistent account of the existing data.

The experimental task of evaluating the various proposed models is complicated by the complexity of reactions which occur when the projectile energy is well above the interaction barrier. Previous studies[6–8] in the vicinity of $E/A \approx 20$–50 MeV have shown that the collision stage produces a broad distribution of multibody final states characterized by continuous energy and momentum distributions. Because inclusive data for particles emitted in these reactions represent an average over many sources, measurements of a more exclusive nature must be performed in order to obtain a meaningful description of the source properties.

In the present work we have performed measurements of light-charged-particle (LCP) spectra tagged by the longitudinal linear momentum transfer (LMT) from the projectile to target nucleus in the interaction of 150-MeV ^{6}Li ions with ^{238}U. The choice of ^{6}Li as a projectile was motivated by two factors. First, ^{6}Li is a transitional nucleus between light-ion and heavy-ion projectiles. Hence, such data contribute to a broader understanding of the systematic dependence of LCP emission on projectile type in intermediate-energy reactions. Second, the loosely-bound cluster structure of ^{6}Li permits the study of projectile fragmentation processes with relatively few breakup channels, most of which are readily separable. By performing exclusive measurements, it is possible to investigate the relationship between the properties of the transferred cluster and the breakup process that has occurred.

Previous inclusive investigations of ^{6}Li-induced reactions in complex nuclei at energies well above the interaction barrier have examined the properties of both projectilelike and targetlike products.[9–11] These studies have demonstrated that even at the relatively low energy of $E/A = 16$ MeV, significant contributions from nonequilibrium processes are present. Exclusive measurements of products of ^{6}Li-induced reactions on a wide range of target nuclei at an incident energy of 75 MeV have been performed with particle-gamma and particle-particle coincidence methods (see Ref. 9 and references therein). These measurements established that reactions with ^{6}Li ions well above the Coulomb barrier are dominated by the ^{2}H-^{4}He cluster structure of the projectile; the primary reaction channels involved either inelastic scattering of ^{6}Li followed by breakup into ^{2}H and ^{4}He, or optimum Q-value absorptive breakup in which a ^{2}H or ^{4}He is absorbed with the remainder of the projectile escaping with beam velocity into the continuum. In addition, these results have suggested that neutron transfer to the target followed by breakup of the excited ^{5}Li contributes significantly to the yields of ^{4}He and protons emitted at forward angles. Further, ^{3}H and ^{3}He emission were found to result primarily

from optimum Q-value transfer.

Here we report inclusive measurements of the linear momentum transfer distribution along with angular distributions and energy spectra for ^{1}H, ^{2}H, ^{3}H, ^{3}He, and ^{4}He, tagged by the corresponding LMT for 150-MeV ^{6}Li-induced reactions on ^{238}U. Linear momentum transfer properties have been determined from measurements of the angle between binary fission fragments (see Ref. 6 and references therein). For this system the total reaction cross section is expected to be equal to the fission cross section, since the system will undergo fission regardless of the collision mechanism. In addition, the average LCP multiplicity is expected to be of the order of one.[10] Thus, although the experiment is not kinematically complete for LCP multiplicity greater than one, the probability for reconstruction of the total momentum balance is still large at this energy.

In Sec. II the experimental details are discussed. The data-analysis procedures and discussion of the experimental results are presented in Sec. III and Sec. IV, respectively. In these sections linear momentum transfer and complex fusion probabilities for ^{6}Li are compared with data for other projectiles. Also, evidence is presented for three primary mechanisms of LCP production: (1) inelastic scattering or single nucleon transfer, (2) optimum Q-value transfer to the target, and (3) emission associated with complete linear momentum transfer. Conclusions are presented in Sec. V.

II. EXPERIMENTAL PROCEDURES

The experiment was performed in the 162-cm diameter scattering chamber at the Indiana University Cyclotron Facility using a beam of 150-MeV ^{6}Li ions. Typical beam currents were 10—20 nA and the beam spot size was less than 3 mm in diameter. Because of the need to maintain high angular precision, the axial stability of the beam position was monitored periodically with a scintillator. In addition, two detectors for elastically scattered ^{6}Li ions were positioned symmetrically with respect to the beam axis at forward angles in order to provide an on-line monitor of possible drifts in the beam position. The target consisted of 550 $\mu g/cm^2$ $^{238}UF_4$ evaporated onto a 100 $\mu g/cm^2$ carbon backing foil and was oriented at an angle of 35 deg with respect to the beam axis throughout the experiment.

The experimental apparatus and definition of detector angles is shown schematically in Fig. 1. The linear momentum transfer distribution was derived from the angle between coincident binary fission events, θ_{AB}. The two fission fragments were detected in an x-y position-sensitive multiwire chamber (MWC) and an x-position sensitive surface barrier detector (PSD) of dimensions 6 mm $\times$ 50 mm. The multiwire chamber had an active area of 14 cm $\times$ 14 cm and was positioned 25 cm from the target. The MWC consisted of two position-sensitive wire planes and a cathode foil between them. Standard delay-line readout was used to obtain position information from both wire planes. The cathode foil was made of 80-$\mu g/cm^2$-thick polypropylene with 30 $\mu g/cm^2$ of silver evaporated on both sides. Both wire planes were grounded and -800 V was applied to the cathode. The gap between the foil and each of the wire planes was 4 mm, while the wire spacing was 1 mm. Position resolution was better than 1 mm, corresponding to an angular resolution of 0.3 deg. Isobutane at a pressure of 8 Torr was used as the working gas. Typical position spectra are shown for coincident fission spectra in Figs. 2(a) and (b).

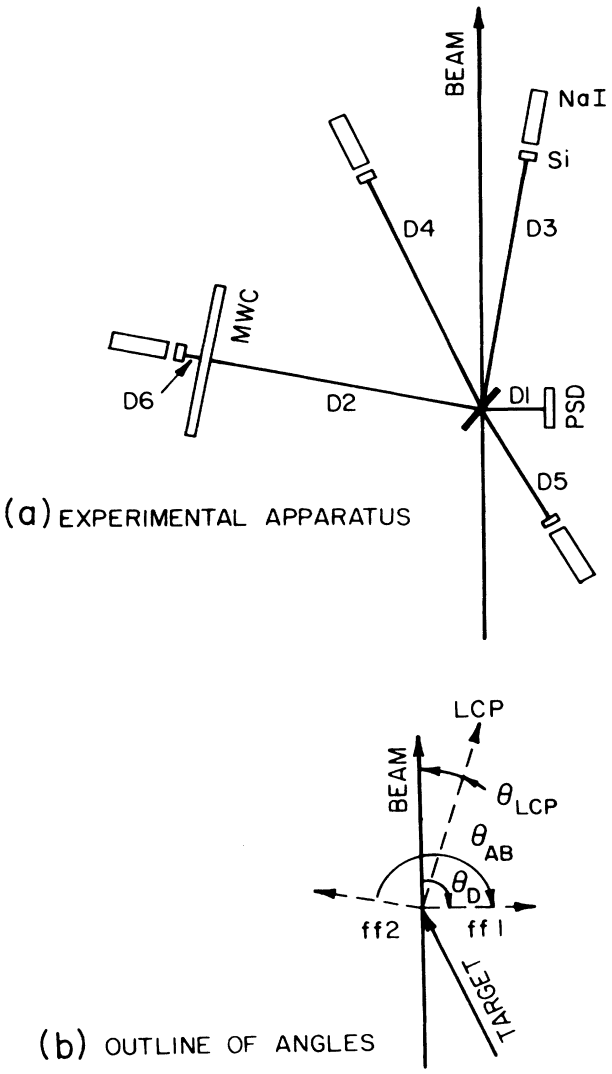

FIG. 1. Schematic diagram of experimental arrangement: (a) physical orientation of detectors includes silicon position-sensitive detector (PSD), position-sensitive multiwire chamber (MWC), and four LCP detector telescopes consisting of a Si ΔE element and a NaI E element; (b) definition of detector angles for fission fragment defining detector (θ_D), fission-fragment opening angle (θ_{AB}), and LCP telescope angle (θ_{LCP}).

The PSD was positioned with its center at 90 deg. The MWC was positioned on the opposite side of the beam axis with its center at -75 deg. The relative angle be-

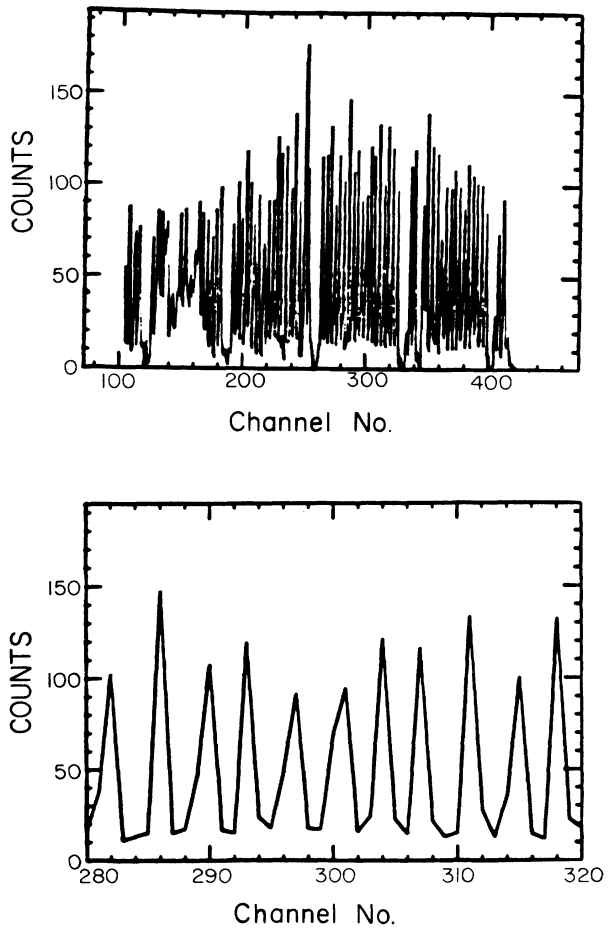

FIG. 2. An example of the x-position spectrum in the wire chamber used in this work (ungated). The upper spectrum shows the entire electrode, with wires of the position-calibration mask visible as wide gaps. The lower spectrum shows a small part of the upper spectrum. Peaks correspond to single wires.

tween these two detectors was mechanically fixed, and hence the 165 deg separation angle remained constant throughout the experiment. The PSD was placed 6.5 cm from the target and had an angular resolution of 0.75 deg. Angular calibrations were carried out with a 13-slit calibration mask. This yielded an overall angular resolution of 0.80 deg for the folding angle between two fission fragments.

Light-charged particles were detected with an array of four $\Delta E/E$ particle identification telescopes which were placed on a table which moved independently of the MWC and PSD. The ΔE elements were 400 μm thick, 200 mm^2 area silicon surface barrier detectors, and the E detectors consisted of NaI detectors of diameter 2.5 cm and thickness 7 cm. Two telescopes were placed at forward angles, a third at an intermediate angle (behind the MWC), and a fourth at a backward angle. Energy calibration of the telescopes was performed with the 150-MeV ^{6}Li beam, using elastic scattering on CH_2 and CD_2 targets. Additional calibrations with a pulser and radioactive sources were performed after the run.

III. DATA ANALYSIS

The longitudinal component of the velocity vector of the fissioning nucleus, $\mathbf{V}_{FN}$, following precompound processes but prior to statistical particle decay, can be determined directly from measurement of the folding angle between binary fission fragments plus the fragment velocities (or kinetic energies). Since for actinide target nuclei the mass loss prior to fission is generally small relative to that of the compound system, one can assume to a good approximation that the linear momentum transferred to the fissioning nucleus is given by $\mathbf{p}_{FN} \cong M_{CN}\mathbf{V}_{FN}$, where M_{CN} is the sum of the target plus projectile masses. Statistical particle emission (primarily neutrons), which either precedes or follows fission, does not affect the average magnitude of $\mathbf{V}_{FN}$, since these particles are assumed to be emitted isotropically in the center-of-mass system. However, statistical particle emission does introduce a significant dispersion in the observed folding angle for a given linear momentum transfer, which serves to reduce the sensitivity of the technique.[6]

Because the present measurements measure neither the fragment velocities nor their kinetic energies, several assumptions are required to derive linear momentum transfer distributions from the measured folding angle θ_{AB}. These assumptions and their expected influence on the experimental results are as follows:

(i) The most probable total kinetic energy release is based on the predictions of fission systematics.[12]

(ii) The mass and kinetic energy distributions are assumed to be symmetric. Previous measurements[13] of ^{238}U fission induced by 140-MeV ^{4}He ions have shown that for this system the mass and energy distributions are Gaussian with a mass width of approximately ± 50 mass units. In order to investigate the influence of asymmetric mass splits on our results, the fission folding angle for full momentum transfer has been calculated under two different assumptions: (1) symmetric mass and energy division (both fragments with $A=122$) and the most probable total E_K given by systematics or (2) a square fission fragment mass distribution centered at $A=122$ with a width of 60 mass units and a kinetic energy distribution corresponding to the predicted most probable value, corrected for mass asymmetry. In the former case the calculated folding angle is 163.8 deg, compared to 163.5 deg for the latter. This difference corresponds to approximately 2.5 percent of the beam momentum and depends nearly linearly on the fraction of beam momentum transferred. Therefore, the momentum transfer correction for mass asymmetry is less than this value for most of the data discussed here. In the analysis of our inclusive results, the momentum transfer distribution includes a correction for this effect, based upon the square mass distribution described above.

(iii) The transverse component of $\mathbf{V}_{FN}$ is taken to be negligible relative to the longitudinal component; i.e., $p_\perp \ll p_{||}$ and $p_{FN} \cong p_{||}$. Since the largest values of $p_\perp$ are associated with peripheral processes, where the linear momentum transfer is low, the major part of the linear momentum transfer distribution is perturbed negligibly by this assumption. It is stressed here that the fission

folding-angle/light-ion coincidence technique can only serve to identify the reaction mechanism if a two-body final state (fissioning system + LCP) is produced in the exit channel. Hence, in more complex precompound interactions we can only determine missing momentum. Uncertainties due to (i), (ii), and (iii) are included in the quoted experimental errors.

(iv) As mentioned above, neutron evaporation does not affect the average value of the folding angle for a given momentum transfer. It does, however, influence the width of the folding angle distribution. Since the width is dependent on the number of neutrons emitted, or excitation energy, this broadening is expected to be most visible for events corresponding to large linear momentum transfers. The magnitude of this effect can be estimated by examining the out-of-plane width of the folding-angle distribution at the folding angle corresponding to complete LMT, where by definition $V_\perp = 0$ for the fissioning nucleus prior to neutron emission. It is found that the out-of-plane folding angle distribution at full momentum transfer accounts quite well for the in-plane distribution of folding angles corresponding to momentum transfers greater than the beam momentum. Hence, no corrections are introduced for this effect; however, it is taken into account in estimating the probability for complete fusion in this system.

IV. EXPERIMENTAL RESULTS

A. Inclusive measurements

The inclusive folding-angle distribution for binary fission fragments is shown in Fig. 3. Also indicated on the figure is the corresponding value of $p_{||}/p_{\text{beam}}$, where $p_{||}$ and p_{beam} denote the longitudinal linear momentum transfer and the beam momentum, respectively. The kinematic transformation from folding angle to $p_{||}$ assumes symmetric fission of the composite target-projectile system and the total kinetic energy release predicted by systematics.[12] Calculations of $p_{||}$ for the exclusive measurements described in Sec. IV B also include corrections for the effects of the coincident light particles on the kinematics. Also shown in Fig. 3 are the most probable folding angles for absorptive breakup involving capture of various substructures of the ^{6}Li projectile (α,d,p,n), with the remainder continuing with the beam velocity.

The experimental results indicate a broad distribution of linear momentum transfers in which the most probable events occur at about 85% of the beam momentum. This corresponds to an average emission of one prompt nucleon during the interaction. A shoulder is also observed near $p_{||}/p_{\text{beam}} \approx 0.3$, roughly equivalent to capture of a deuteron accompanied by a beam-velocity ^{4}He ejectile.

From the data shown in Fig. 3 we have determined the following quantities:

(1) The most probable value of the linear momentum transfer, $p_{||}^{mp}$—this quantity is most relevant to the properties of central collisions, at least at beam energies below $E/A = 50$ MeV.

(2) The average value of the linear momentum transfer distribution, $\langle p_{||} \rangle$—for U targets this quantity has the advantages of defining the total reaction cross section in the energy domain studied here and of unambiguous definition. Peripheral interactions are included in the average LMT; hence, this quantity depends on the fissility of the decaying nucleus, since low deposition energy processes may not lead to fission for targets lighter than the actinides.

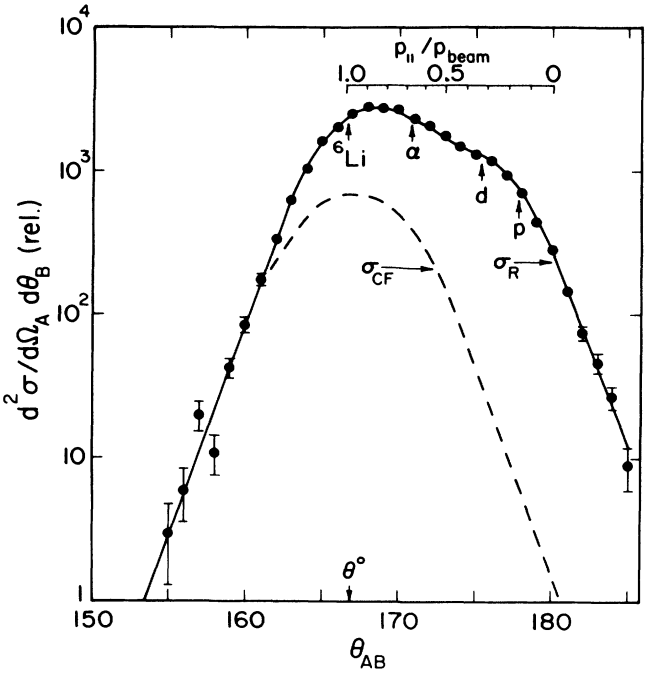

FIG. 3. Inclusive fission-fragment folding-angle distribution for 150 MeV ^{6}Li incident on ^{238}U. All nonplanar events have been projected onto the reaction plane. The upper scale involves kinematic transformation to a momentum transfer scale, $p_{||}/p_{\text{beam}}$, assuming symmetric fission and fission fragment kinetic energies predicted by kinematics. Momentum transfers corresponding to transfer of ^{6}Li, α, d, and p to the target nucleus are marked by arrows. The angle θ° (indicated by arrow) corresponds to the most probable folding angle for complete fusion, corrected for mass asymmetry of the fission fragment mass distribution. The dashed line represents the upper limit to the complete fusion cross section, derived from the out-of-plane folding angle distribution at θ° as described in text.

(3) An *upper limit* for the ratio σ_{CF}/σ_R, where σ_{CF} and σ_R denote complete fusion and total reaction cross sections, respectively. In deriving σ_{CF}/σ_R the complete fusion component has been approximated by the out-of-plane (ϕ) distribution at the folding angle calculated for complete fusion (i.e., $p_{||}/p_{\text{beam}} = 1.0$), corrected for the effects of mass/energy asymmetry for the fission fragments, as discussed in Sec. III. This is given by the dashed line in Fig. 3. Because of the significant yields of nonequilibrium light particles at these energies, the concept of complete fusion becomes increasingly ambiguous above $E/A \simeq 10$–15 MeV and only upper limits for σ_{CF}/σ_R can be derived.

In Table I and Fig. 4, we present the above quantities as

TABLE I. Properties of linear momentum transfer distributions for the $^{6}Li + ^{238}U$ system at bombarding energies near the Fermi energy. Data at $E/A=30$ and 35 MeV are from Ref. 20. Symbols are defined in text.

	E/A		
	25 MeV	30 MeV	35 MeV
p_{beam} (MeV/c)	1300	1420	1540
$[(E-V)/A]^{1/2}$ (MeV$^{1/2}$)	4.47	5.00	5.48
$p_{\|\|}^{mp}$ (MeV/c)	1090	1140	1100
$p_{\|\|}^{mp}/A$ (MeV/c)	182	190	183
$p_{\|\|}^{mp}/p_{beam}$	0.84	0.80	0.72
$\langle p_{\|\|} \rangle$ (MeV/c)	970	990	960
$\langle p_{\|\|} \rangle/A$ (MeV/c)	162	165	160
$\langle p_{\|\|} \rangle/p_{beam}$	0.75	0.69	0.62
σ_{CF}/σ_R	0.23±0.04	0.20±0.04	0.16±0.04
Out-of-plane width at $p_{\|\|}=p_{beam}$ (deg)	8.0 ±0.4	9.2 ±0.5	10.0 ±0.5

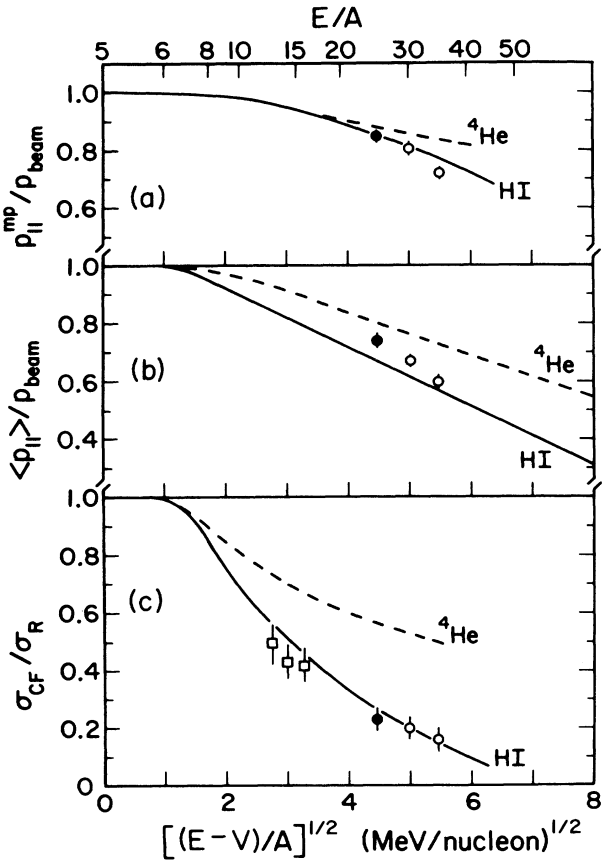

FIG. 4. (a) Most probable momentum transfer relative to the beam momentum, $p_{||}^{mp}/p_{beam}$; (b) the average momentum transfer relative to the beam, $\langle p_{||} \rangle/p_{beam}$; and (c) the upper limit for the ratio of the complete fusion cross section to the total reaction cross section, all plotted as a function of the beam velocity above the Coulomb barrier (lower scale) and E/A (upper scale). Solid circles are the present data, open circles are from Ref. 20, and open squares are averages of these values for slightly lighter target nuclei from Ref. 10. Solid lines summarize values for heavy ions (^{12}C-^{40}Ar) and the dashed lines represent the data for ^{4}He ions.

a function of beam energy E/A (upper scale) and the beam velocity parameter $[(E-V)/A]^{1/2}$ (lower scale), where V is the Coulomb barrier. Also included in Fig. 4 are $E/A=30$ and 35 MeV, reported elsewhere,[14] and lower-energy values of σ_{CF}/σ_R for ^{6}Li reactions with nuclei in the Au-Pb region reported by Vigdor *et al.*[10] Since one of the objectives of this research has been to investigate the behavior of the loosely-bound ^{6}Li projectile relative to tightly-bound ^{4}He ions and heavier ions, we have also presented data for these projectiles in Fig. 4 for comparative purposes.[13–15]

In terms of the most probable momentum transfer and the complete fusion probability, which reflect the central collision properties of these interactions most closely, the ^{6}Li projectile behaves very similarly to the heavy-ion projectiles. In the case of the average momentum transfer, $\langle p_{||} \rangle$, ^{6}Li exhibits behavior intermediate between ^{4}He ions and heavy ions. This result can most probably be understood as being due to the increased number of open channels for projectile fragmentation and absorptive breakup with increasing projectile mass. In this respect the strong enhancement of absorptive breakup involving ^{4}He capture (Sec. IV B) serves to produce larger values of $\langle p_{||} \rangle$ for ^{6}Li relative to heavier projectiles in which ^{4}He capture represents a much smaller fraction of the beam momentum.

In Fig. 5 we plot the linear momentum transfer *per projectile nucleon* as a function of beam E/A and velocity. Here the solid line represents the expected result for full momentum transfer, the upper dashed line summarizes the most probable momentum transfer for ^{12}C and ^{14}N projectiles[8,14], and the lower dashed curve represents the average momentum transfer for the same data. Relative to other projectiles the ^{6}Li data exhibit the same behavior as in Fig. 4. One observes that the linear momentum transfer per nucleon reaches a maximum limiting value, $p_{||}^{max}/A$, near a projectile energy of $E/A=30$ MeV, somewhat lower than for ^{4}He and heavier ions, where this maximum occurs nearer $E/A \approx 35$ MeV.[14] This shift is attributed to the loosely-bound structure of ^{6}Li, which enhances the probability for momentum loss due to pro-

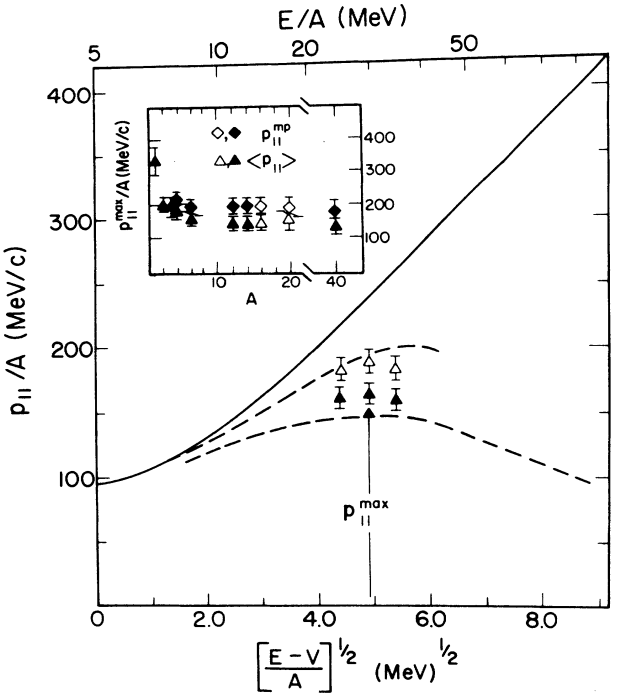

FIG. 5. Momentum transfer per nucleon for ^{6}Li projectiles of $E/A=25$, 30, and 35 MeV/A. Solid triangles are for average momentum transfer per nucleon and open triangles for the most probable values. The dashed lines show the behavior of these values for ^{12}C and heavier ions; the upper curve corresponds to $p_{||}^{mp}$ and the lower curve to $\langle p_{||} \rangle$. The arrow indicates the deduced maximum value of the momentum transfer as a function of beam E/A. These values are plotted in the insert to the figure for several projectiles ranging from protons to ^{40}Ar.

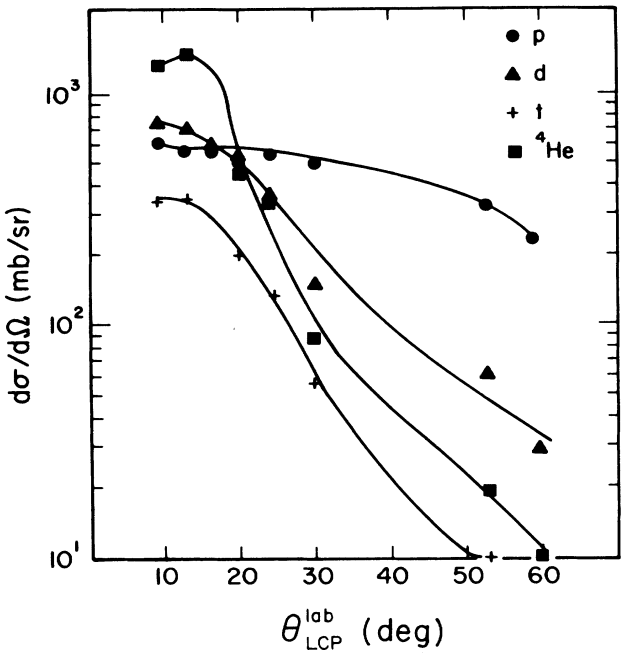

FIG. 6. Angular distributions for p (●), d(▲), t (+), and ^{4}He (■) ejectiles in coincidence with angle-correlated fission fragments.

jectile fragmentation processes. The values of the limiting momentum transfer per nucleon, $p_{||}^{max}/A$, for ^{6}Li are compared with other projectiles, ranging from protons to ^{40}Ar, in the inset of Fig. 5. It is found that for all but the lightest ions this value is a constant, corresponding to maximum values of $p_{||}^{mp}/A$ of $\approx$200 MeV/c and $\langle p_{||} \rangle \approx 150$ MeV/c. This indicates a commonality of mechanisms which describes the global characteristics of momentum loss in collisions between complex nuclei. It has been suggested that nonequilibrium light-particle emission is the major source of momentum loss, and in the following subsection we investigate these processes in greater detail.

B. Light-charged particle coincidence studies

In order to investigate the mechanisms which limit linear momentum transfer in the ^{6}Li + ^{238}U system, the angular and energy distributions of H and He ejectiles have been measured in coincidence with angle-correlated fission fragments.

1. Angular and energy spectra

In Fig. 6 the angular distributions are shown for energy-integrated yields of p, d, t, and ^{4}He ions emitted in coincidence with binary fission events. No constraints are placed on the fission-fragment folding angle. The angular distributions for all complex ejectiles are observed to peak near the classical grazing angle for this reaction, $\theta_{gr} \cong 13$ deg, and then decrease rapidly with increasing angle. This behavior indicates that these particles are associated with projectile fragmentation processes, an assumption that is reinforced by examination of the corresponding linear momentum transfer values, as discussed later in the text.

The emission of ^{4}He ions dominates the angular distributions at forward angles, thus accounting for a major fraction of the momentum loss for peripheral processes. In contrast, the angular dependence of the proton yield is much weaker than the complex projectiles, and beyond an angle of 25 deg, protons constitute the major contributor to the light-charged particle yield. Hence, the emission of nucleons appears to be associated (at least in part) with more central collisions. Support for this inference demands examination of both the energy spectra of the light ejectiles and the linear momentum transfer associated with the targetlike fragment. Integration of the angular distributions yields the total cross sections for $Z=1$ and 2 isotopes listed in Table II. Because of the thickness of our ΔE detectors, the evaporation component of the ^{4}He spectra is not included ($E_\alpha < 28$ MeV).

Energy spectra for coincident light-charged particles are shown in Fig. 7 for angles of 9, 59, and 149 deg. For all projectiles the forward-angle spectra (9 deg) are peaked at the beam velocity. This fact and the previously mentioned angular distributions are taken to be evidence for projectile fragmentation and absorptive breakup as the

TABLE II. Total cross sections for light-charged particles in coincidence with angle-correlated fission fragments in the 150 MeV $^{6}Li + ^{238}U$ reaction. Evaporation component ($E \leq 28$ MeV) is not included for ^{4}He due to ΔE detector thickness.

	^{1}H	^{2}H	^{3}H	^{4}He
σ (mb)	2200±300	720±110	260±40	≥550±80

primary mechanism for producing these forward-angle light ions. However, while the widths of the deuteron and alpha-particle spectra correspond well with the predictions of a simple fragmentation picture,[16] the widths of the proton, triton, and ^{3}He spectra are significantly broader. For example, the intrinsic momentum width σ_0 for both d and α spectra yields identical values of $\sigma_0 \approx 80$ MeV/c, in good agreement with systematics for projectile fragmentation.[16] On the other hand, for protons the spectra yield $\sigma_0 = 120$ MeV/c and for ^{3}H and ^{3}He ejectiles, $\sigma_0 \geq 110$ MeV/c. A possible explanation for this observation may be that sequential decay processes also are important contributors to p, t, and ^{3}He formation.

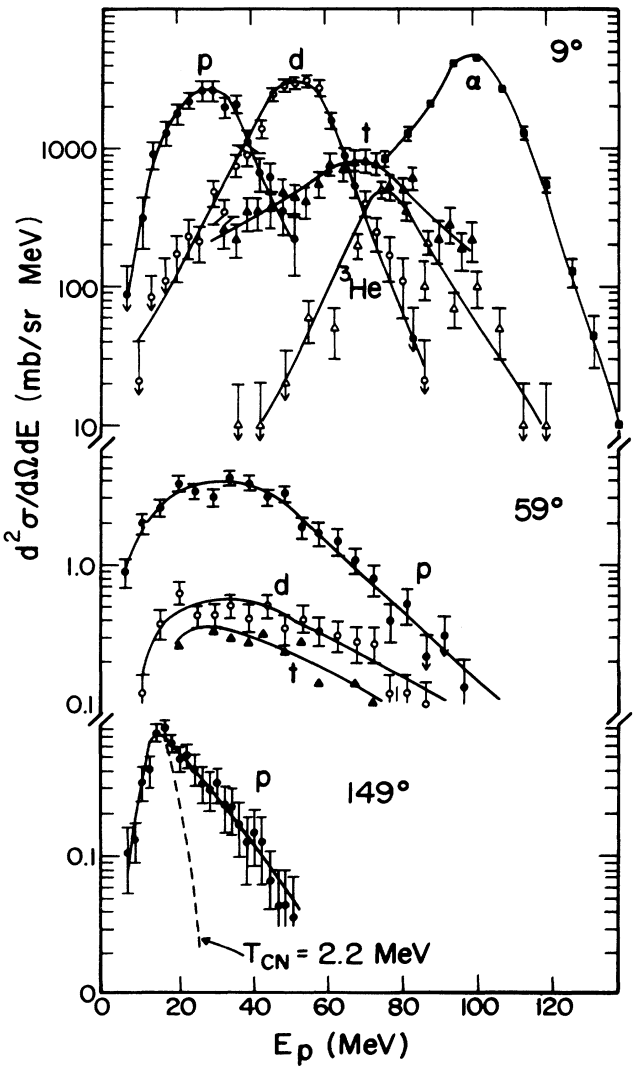

FIG. 7. Energy spectra for LCP ejectiles in coincidence with angle-correlated fission fragments at several angles: (a) 9 deg, (b) 59 deg, and (c) 149 deg. Ejectile type is indicated by (●) for ^{1}H, (○) for ^{2}H, (▲) for ^{3}H, (△) for ^{3}He, and (■) for ^{4}He. In part (c) the solid line represents a Maxwellian fit to the spectra, and the dashed line is the result of an evaporation calculation assuming a completely equilibrated compound nucleus.

None of the forward-angle spectra, with the possible exception of protons, show any important relative contribution due to central collisions, for which a Maxwellian energy distribution peaked near the Coulomb barrier (~10—15 MeV) is expected. The high-energy tail for protons is suggestive of such a source, but the difference between the beam-velocity energy (E/A) and the Coulomb barrier is too small to provide a convincing case. Finally, the small difference in the ejectile energy corresponding to the peak heights for the t and ^{3}He spectra is consistent with the difference of about 10 MeV in the Q value for ^{3}H and ^{3}He transfer.

At the more backward angles the character of each spectrum evolves toward a Maxwellian distribution with a significant high-energy tail, extending up to 100 MeV for ^{1}H ions at 59 deg. Yields for energetic He ions are negligible beyond 30 deg, and only protons are observed beyond an angle of 60 deg. Even at the backwardmost angle of 149 deg, protons are observed with an E/A value up to twice that of the beam. Given these characteristics, central collisions appear to be the most probable source for the light-charged particles emitted at large angles. This is confirmed by the linear momentum characteristics of the targetlike residue, as discussed below.

2. *Associated linear momentum transfer distributions*

Figures 8 and 9 show the linear momentum transfer distributions ($p_{||}/p_{beam}$) for fission fragments in coincidence with protons and with deuterons, tritons, and alpha particles, respectively. The $p_{||}/p_{beam}$ scale is calculated for the same assumptions as applied previously to the inclusive data and do not include the linear momentum component of the light ejectile. In the proton plots a gate has been placed on the particle energy which divides the spectrum into two approximately equal components, one corresponding to protons with energies less than 30 MeV (LE) and the remainder to protons above 30 MeV (HE). From the systematic features of these plots, one obtains an overview of the momentum balance in the $^{6}Li + ^{238}U$ system, which can then be related to specific mechanisms.

a. Proton- and deuteron-gated events. In the proton- and deuteron-gated linear momentum transfer distributions (Figs. 8 and 9), two production mechanisms are apparent. These are most distinct for the low-energy component of the proton-gated spectra at small angles. Here one observes (1) a low momentum transfer component with $p_{||}/p_{beam} \approx 0.2$, corresponding to transfer of one nucleon, and (2) an absorptive breakup component with $p_{||}/p_{beam} \approx 0.75$, corresponding to ^{4}He or ^{5}He capture by the target. In each case it is assumed that the ejectile energy is $E/A \approx 25$ MeV, consistent with the spectra of Fig. 7. The widths of the two peaks are also in good agreement with expectations based upon measurements of folding-angle distributions[13–15] as a function of excitation

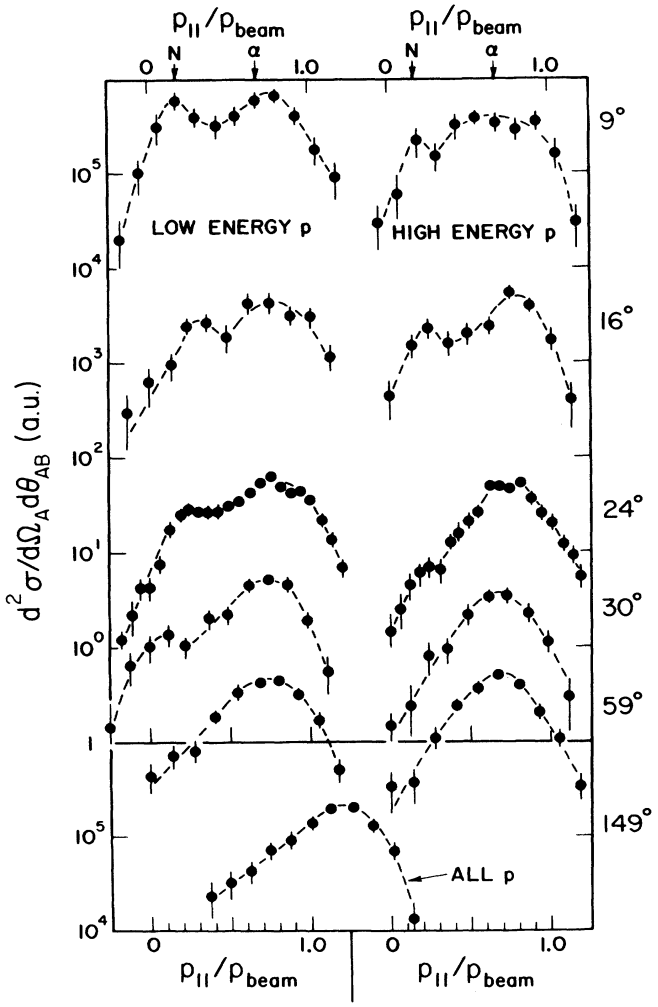

FIG. 8. Fission fragment linear momentum transfer distributions gated on protons at several angles. For forward angles the proton energy spectra are divided into low- and high-energy bins, with the cross section divided approximately equal between the two. At 149 deg all data are binned together. Expected centroids for transfer of a single nucleon and a ^{4}He ion (α) are indicated by arrows.

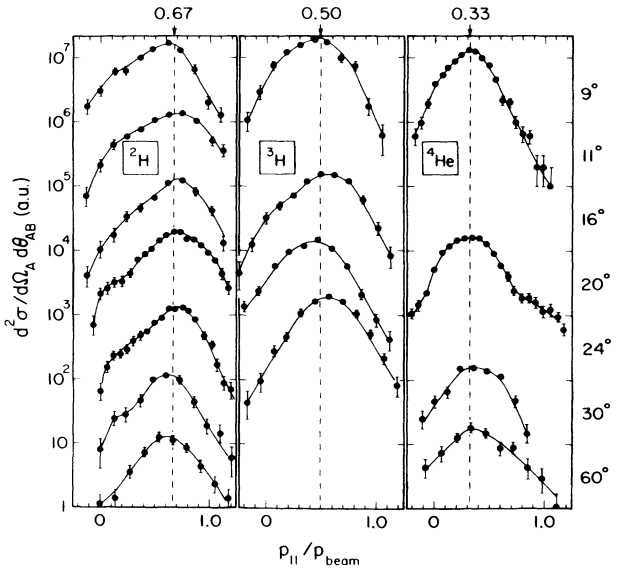

FIG. 9. Fission fragment linear momentum transfer distributions gated on deuterons, tritons, and ^{4}He ions at several angles. Dashed lines represent the expected centroid for transfer of a ^{4}He ion (deuteron spectra),^{3}He (triton spectra), and a ^{2}H (^{4}He spectra).

energy, i.e., about 2.8 deg for $E^* \leq 25$ MeV and 6.0—6.5 deg for $E^* \approx 100$—125 MeV.

For the low momentum-transfer component, one expects the proton yields to have their origin in three projectile fragmentation channels: (^{6}Li$^* \rightarrow \alpha + p + n$; ^{5}Li$^* \rightarrow \alpha + p$, and ^{6}Li$^* \rightarrow \alpha + d^* \rightarrow \alpha + p + n$). All three processes lead to low linear momentum transfers and are not directly distinguishable with our experimental method. Deuteron production in low momentum-transfer events is attributed primarily to ^{6}Li$^* \rightarrow \alpha + d$ breakup on the basis of Q-value considerations. The yield of this low-momentum transfer component decreases rapidly as a function of angle for both protons and deuterons, indicating that it originates in very peripheral reactions. Further, the relative strength of low momentum-transfer events is significantly weaker for the high-energy component of the energy spectra, suggesting that the most energetic LCP's are more closely associated with strong target-projectile interactions.

For both p and d ejectiles the low momentum-transfer component is strongly forward peaked and becomes negligible at angles beyond about 25 deg, or 10 deg beyond the grazing angle. Thus, the low momentum transfer to the target nucleus combined with the forward-peaked angular distribution and beam velocity energies of the ejectiles support a projectile fragmentation mechanism in the field of the target nucleus as a major source of light-charged particles in this reaction. Although our experiment is kinematically incomplete for this case (i.e., the unobserved alpha particle), concidence studies of correlations between light-charged particles in ^{6}Li-induced reactions on lighter targets at lower energies[9] also support the above picture.

For proton and deuteron emission associated with high momentum transfer events, the data of Figs. 8 and 9 appear to provide a nearly completely account of the longitudinal momentum balance. We define the observed momentum relative to that of the beam as

$$R = \frac{\langle p_{||} \rangle_{LCP} + \langle p_{||} \rangle_f}{p_{beam}} ,$$

where $\langle p_{||} \rangle_{LCP}$ is the average longitudinal linear momentum of the light-charged particle and $\langle p_{||} \rangle_f$ is the same value for fission. Hence, $R = 1$ corresponds to a complete accounting of the linear momentum in the reaction; i.e., a light-charged particle multiplicity of one. Values of R for light ions in coincidence with the high linear momentum transfer component are listed in Table III as a function of angle. In each case the high linear momentum transfer

TABLE III. Values of variable R, as defined in text, for several ejectiles at different angles of the light charged particle detector.

θ_{LCP}	^{1}H	^{2}H	^{3}H	^{4}He
9°	0.92±0.1	1.0 ±0.1	0.82±0.15	0.95±0.05
16°	0.82±0.08	1.0 ±0.08	0.89±0.12	1.0 ±0.10
24°	0.80±0.06	1.01±0.07	1.0 ±0.1	
30°	0.81±0.05	0.98±0.06	0.85±0.10	0.90±0.10
59°	0.85±0.05	0.9 ±0.06		
114°	0.95±0.1			
149°	1.0 ±0.1			

component has been defined by fitting a Gaussian function to the data.

The values of R for the deuteron-gated spectra are also consistently equal to 1.0 within errors over the entire angular range. This result confirms that the primary source of deuterons in this reaction is absorptive breakup involving capture of an alpha particle. For protons the forward-angle momentum balance calculations yield an average value of $R=0.84\pm0.06$. Since the missing momentum in this case coincides nearly exactly with the loss of one nucleon, these data indicate that deuteron breakup following absorption of an alpha particle is an important contributor to the proton yields. However, it is noted that at the forwardmost angle ($\theta=9$ deg), the value of $R=0.92$ suggests an admixture of complete momentum transfer with the single nucleon escape mechanism.

Probably the most striking feature of the proton data is found at backward angles, where $R=1.0$. Correspondingly, it is noted in Fig. 8 that the folding-angle data yield $p_{||}/p_{\text{beam}}\approx1.2$, consistent with full momentum transfer fission preceded by emission of an energetic proton in the backward direction. This result confirms that the energetic protons discussed previously in conjunction with Fig. 7 have their origin in central collisions which involve *complete energy and momentum transfer* from projectile to target nucleus.

The mechanism responsible for production of these energetic nucleons—now observed in several systems[10,17,18] as summarized in Table IV—remains a challenging problem in the study of interactions between complex nuclei. Their origin is not of an equilibrium nature, as is illustrated by the results of a statistical calculation performed for the evaporation of protons from a source moving with the compound nucleus velocity and having a temperature corresponding to a fully-equilibrated compound nucleus ($T_{CN}=2.2$ MeV for a level density parameter $a=A/8$ MeV^{-1}). This calculation is shown by the dashed curve in the 149 deg spectrum of Fig. 7. In contrast, a fit to the spectrum with a Maxwellian function which assumes volume absorption yields a temperature parameter of about 7 MeV. Similar observations for lower energy inclusive proton data for ^{6}Li-induced reactions have been reported previously by Vigdor *et al.*[10] A comparison of temperature parameters T extracted from similar fits to backward-angle spectra is summarized in Table IV, which shows the general nature of this phenomenon.

An alternative explanation may lie in Fermi motion effects. To simulate this we have performed an intranuclear cascade calculation using the code CLUST (Ref. 3) to predict the spectra of protons emitted at back angles in the reaction of 150-MeV ^{4}He ions incident on ^{238}U. We choose ^{4}He in place of ^{6}Li because: (1) it is the heaviest projectile for which all experimental scattering cross sections are included in the network of scattering possibilities contained in the code, and (2) it is a tightly-bound projectile that should maximize the effects of Fermi motion on the scattering process (i.e., the breakup probability is small). The choice of total energy, rather than energy per nucleon, was made for the projectile energy in order to overestimate cascade effects relative to expectations for the ^{6}Li projectile. Based on 30 000 cascade events, the calculated cross sections were two orders of magnitude below the data. With these statistics it was not possible to generate energy spectra predicted by the cascade code.

TABLE IV. T_{CN} denotes the temperature of the compound nucleus (assumes $a=A/8$ MeV^{-1}). T denotes the apparent temperature for protons at backward angles ($\theta\geq150°$).

Ref.	Projectile	Energy	E/A	Target	T (MeV)	T_{CN} (MeV)
17	^{1}H	90	90	^{232}Th	8.5	1.76
17	^{2}H	70	35	^{232}Th	7.0	1.55
17	^{4}He	140	35	^{232}Th	6.5	2.18
10	^{6}Li	75	12.5	^{197}Au	3.8	1.72
This work	^{6}Li	150	25.0	^{238}U	7.0	2.22
18	^{16}O	215	13.4	^{197}Au	3.8	2.84
18	^{16}O	310	19.6	^{197}Au	4.4	3.41
18	^{16}O	315	19.7	^{238}Au	4.5	3.15

Thus, it would appear that either the high energy tail of the Fermi distribution in the cascade code must be significantly increased or a more complex mechanism is required for explanation of these energetic light-charged particles associated with complete momentum and energy transfer from the projectile to the composite system.

b. Triton-, ^{3}He-, and ^{4}He-gated events. The linear momentum transfer properties associated with ^{4}He emission (Fig. 9 and Table III) are generally consistent with complete momentum balance ($R=1.0$) involving two-body final states, i.e., fission preceded by emission of one prompt alpha particle. The fission momentum transfer distributions gated on alpha particles, shown in Fig. 9, are representative of these ejectiles. A momentum transfer $p_{||} \approx \frac{1}{3} p_{\text{beam}}$ is found, corresponding to capture of a deuteron from the ^{6}Li projectile. There is also evidence for a shoulder corresponding to a small contribution from single nucleon transfer. The resultant ^{5}Li* or ^{5}He* would then undergo sequential decay to yield ^{4}He + N. This interpretation is also consistent with the proton coincidence data discussed above. From examination of the linear momentum balance for both deuterons and alpha particles, as well as the fragmentation widths, it appears that α-d cluster structure continues to exercise a dominant influence on ^{6}Li-induced reactions at energies near the Fermi energy.

Because of limited statistics the triton- and ^{3}He-gated momentum transfer distributions are more difficult to interpret. For the most part the $A=3$ ejectiles are associated with $p_{||}/p_{\text{beam}}$ values of ≈ 0.4—0.5. Hence, a major fraction of these events can be accounted for by an absorptive breakup process involving capture of three nucleons; i.e., ^{238}U(^{6}Li,^{3}H)^{241}Pu* and ^{238}U(^{6}Li,^{3}He)^{241}Np*. The preference for ^{3}He capture (with ^{3}H as the ejectile), as indicated by the energy spectra data of Fig. 7, appears to be inconsistent with an optimum Q-value transfer mechanism, for which equivalent yields of ^{3}H and ^{3}He might be expected. The results suggest that isospin may also be important in absorptive breakup, since ^{238}U is a neutron-excess nucleus and ^{3}He capture serves to lower the isospin of the system.

The observation of enhanced ^{3}H yields relative to ^{3}He is consistent with lower-energy data, where the ^{3}He/^{3}H ratio is found to be target dependent. For 75 MeV ^{6}Li ions incident on ^{56}Fe (low isospin) this ratio is 0.73, on ^{106}Pd it is 0.50, and on a gold target (high isospin) it is 0.34, roughly the same as our uranium result.[11] The ^{3}He/^{3}H ratio for our data is also strongly angle dependent with small angles yields yielding a low ratio and large angles exhibiting nearly equivalent yields. If small scattering angles are associated with large impact parameters, then this result implies that the most peripheral reactions are influenced most strongly by isospin considerations, favoring ^{3}He capture. With decreasing impact parameter, the increasing strength of the projectile-target interaction leads to a more random probability for three-nucleon capture.

The mechanisms by which ^{3}H and ^{3}He can be produced in collisions for which $p_{||}/p_{\text{beam}} \ll 0.5$ include: $^6\text{Li}^* \rightarrow {}^3\text{H} + {}^3\text{He}$, $^4\text{He}^* \rightarrow {}^3\text{H} + \text{p}$, or $^3\text{He} + \text{n}$; $^7\text{Li}^* \rightarrow {}^3\text{H} + {}^4\text{He}$ and $^7\text{Be}^* \rightarrow {}^3\text{He} + {}^4\text{He}$. The first two mechanisms are strongly Q-value inhibited. In addition, projectile fragmentation of ^{6}Li* or decay of ^{4}He* imply roughly equal ^{3}H/^{3}He yields which are not observed. Thus, the nucleon pickup channels seem to be the best candidates to explain the observed ^{3}H/^{3}He ratios. Further, these low momentum-transfer events are primarily associated with the beam velocity $A=3$ ejectiles, which would be expected for the nucleon-pickup channel. Of the two pickup possibilities, isospin considerations would favor the neutron pickup channel, leading to an enhanced ^{3}H/^{3}He ratio as observed. A similar effect has been previously observed in bombardments of ^{90}Zr with 95-MeV ^{6}Li ions.[19]

V. CONCLUSIONS

These measurements have sought to elucidate the principal mechanisms of momentum loss in collisions between a loosely-bound complex projectile, ^{6}Li, and ^{238}U at intermediate energies. From inclusive studies it is found that at the same E/A, the central collision properties of ^{6}Li, as defined by the most probable momentum transfer and complete fusion cross sections, are essentially identical to those of heavy-ion projectiles ranging from ^{12}C to ^{40}Ar. The average momentum transfer for ^{6}Li, which includes the effects of peripheral reactions, is intermediate between ^{4}He and heavy-ion projectiles. This behavior can be understood in terms of deuteron and alpha particle absorptive breakup processes. As in the case for ^{12}C and heavier projectiles, the momentum transfer per projectile nucleon reaches a maximum value corresponding to $p_{||}^{mp}/A \approx 200$ MeV/c and $\langle p_{||} \rangle / A \approx 150$ MeV/c. The maximum occurs at a bombarding energy $E/A \simeq 30$ MeV, slightly lower than for ^{4}He and heavier ions where this peak occurs in the vicinity of $E/A \approx 35$—40 MeV. This behavior is attributed to the fragile nature of the ^{6}Li nucleus.

Exclusive studies have provided a characterization of the major sources of momentum loss in these reactions. The forward-angle spectra, presumably indicative of peripheral interactions, are dominated by deuterons and alpha particles. These ejectiles exhibit energy spectra peaked at the beam velocity and the momentum balance measurements demonstrate that they originate primarily from two-body final states (i.e., the fissioning nucleus and one LCP). These factors argue strongly for a peripheral absorptive breakup mechanism as the primary source of these LCP's. Further, the momentum widths ($\sigma_0 \simeq 80$ MeV/c) of the d and α spectra are in good agreement with the systematics of projectile fragmentation. For ^{1}H, ^{3}H, and ^{3}He ejectiles the data indicate that an admixture of both inelastic and absorptive breakup mechanisms contributes to the LCP yields, in some cases accompanied by sequential decay of the primary fragments. These conclusions are supported by a momentum balance analysis, which demonstrates the existence of missing momentum for these LCP's. In addition, the momentum widths for these ejectiles are 40—50 percent larger than for ^{2}H and ^{4}He.

Beyond the grazing angle most of the LCP yield is accounted for by proton emission. The backward-angle energy spectra are Maxwellian in shape and originate from high linear momentum transfer collisions; for angles

greater than 90 deg, complete linear momentum transfer is observed. The most notable feature of these proton spectra is the high slope temperatures associated with the exponential tail of the Maxwellian distributions. Assuming volume emission, an apparent temperature of $T=7$ MeV is derived for protons originating from full momentum transfer events at 149°. This is in sharp contrast to the temperature expected for compound nucleus formation in the 150 MeV ^{6}Li reactions, i.e., $T_{CN}=2.2$ MeV (assuming $a=A/8$ MeV^{-1}). This result establishes the fact that these high-energy backward protons have their origin in central collisions in which nearly all of the beam momentum is transferred to the struck nucleus. This behavior cannot be accounted for by intranuclear cascade calculations.[3] Clearly this phenomenon warrants further experimental and theoretical investigation.

In summary, these data indicate that momentum loss in intermediate energy collisions can be accounted for primarily by fast nucleon emission for central collisions and a combination of inelastic and absorptive breakup processes, including sequential decay of the ejectile, for peripheral interactions. Currently, theoretical calculations which incorporate all these mechanisms into the reaction dynamics do not exist. It remains a significant challenge for reaction theory to account for exclusive data of this sort in the future.

ACKNOWLEDGMENTS

The authors wish to acknowledge Dennis Friesel and the IUCF operating crew for providing the ^{6}Li beams in this experiment; Bill Lozowski for fabrication of the ^{238}U targets; Terry Sloan for assistance with the scattering chamber hardware, and N. R. Yoder for his help in software development for data analysis. We thank W. Friedman, C. K. Gelbke, and W. G. Lynch for discussions concerning these data. This work was supported by the U.S. Department of Energy (Contract No. DE-AC02-81ER-40007) and the National Science Foundation (Grant NSF PHY 8114339/05).

*Present address: Department of Physics and Astronomy, University of North Carolina, Chapel Hill, NC 27514.
†Present address: Bukietowa 68, Warsaw, Poland.
‡Present address: TRIUMF, Vancouver, British Columbia, Canada.

[1]M. Blann, Annu. Rev. Nucl. Sci. **25**, 123 (1975); Phys. Rev. C **31**, 1245 (1985).
[2]K. Chen, Z. Fraenkel, G. Friedlander, J. R. Grover, J. M. Miller, and Y. Shimamoto, Phys. Rev. **166**, 949 (1968).
[3]G. J. Mathews, B. G. Glagola, R. A. Moyle, and V. E. Viola, Phys. Rev. C **25**, 2181 (1982).
[4]D. H. Boal, Phys. Rev. C **25**, 3068 (1982).
[5]W. A. Friedman and W. G. Lynch, Phys. Rev. C **28**, 16 (1983); **28**, 950 (1983).
[6]V. E. Viola, B. B. Back, K. L. Wolf, T. C. Awes, C. K. Gelbke, and H. Breuer, Phys. Rev. C **26**, 178 (1982).
[7]M. B. Tsang, D. R. Klesch, C. B. Chitwood, D. J. Fields, C. K. Gelbke, W. G. Lynch, H. Utsonomiya, K. Kwiatkowski, V. E. Viola, and M. Fatyga, Phys. Lett. **134B**, 169 (1984).
[8]W. G. Meyer, V. E. Viola, R. G. Clark, R. Theus, and S. M. Read, Phys. Rev. C **20**, 1716 (1979).
[9]C. M. Castaneda, H. A. Smith, P. P. Singh, and H. J. Karwowski, Phys. Rev. C **21**, 179 (1980).
[10]S. E. Vigdor, H. J. Karwowski, W. W. Jacobs, S. Kailas, P. P. Singh, F. Soga, and T. G. Throwe, Phys. Rev. C **26**, 1035 (1982).
[11]J. Jastrzebski, H. J. Karwowski, M. Sadler, and P. P. Singh, Phys. Rev. C **19**, 724 (1979).
[12]V. E. Viola, K. Kwiatkowski, and M. Walker, Phys. Rev. C **31**, 1550 (1985).
[13]V. E. Viola, C. T. Roche, W. G. Meyer, and R. G. Clark, Phys. Rev. C **10**, 2416 (1974).
[14]M. Fatyga, K. Kwiatkowski, V. E. Viola, C. B. Chitwood, D. J. Fields, C. K. Gelbke, W. G. Lynch, J. Pochodzalla, M. B. Tsang, and M. Blann, Phys. Rev. Lett. **55**, 1376 (1985).
[15]F. Saint-Laurent, M. Conjeaud, R. Dayras, S. Harrar, H. Oeschler, and C. Volant, Nucl. Phys. **A422**, 307 (1984).
[16]R. G. Stokstad, Comments Nucl. Part. Phys. (to be published).
[17]J. R. Wu, C. C. Chang, and H. D. Holmgren, Phys. Rev. C **19**, 370 (1979); **19**, 659 (1979).
[18]T. C. Awes *et al.*, Phys. Rev. C **24**, 89 (1981); **25**, 2361 (1982)
[19]S. E. Vigdor, C. Casteneda, H. J. Karwowski, P. P. Singh, H. A. Smith, and J. D. Wiggins, Indiana University Cyclotron Facility Scientific and Technical Report, 1978, p. 74.
[20]M. Fatyga, K. Kwiatkowski, V. E. Viola, C. B. Chitwood, D. J. Fields, C. K. Gelbke, W. G. Lynch, J. Pochodzalla, and M. B. Tsang, Indiana University Report INC-40007 32, 1985.